

# Multiple-gap structure in electric-field-induced surface superconductivity

Yousuke Mizohata, Masanori Ichioka, and Kazushige Machida  
*Department of Physics, Okayama University, Okayama 700-8530, Japan*  
(Dated: January 7, 2013)

Local superconducting gap structure is studied as a function of nanoscale depth in electric-field-induced surface superconductivity such as in SrTiO<sub>3</sub>. We examine solutions of Bogoliubov-de Gennes equation in two limiting confinement potential cases of electric field with and without screening effects. As unique properties different from bulk superconductivity, there appear in-gap states even for isotropic *s*-wave pairing, due to multiple gap structure of sub-band dependent surface superconductivity. These determine the depth-dependence of local superconductivity.

PACS numbers: 74.78.-w, 73.20.At, 74.20.Pq, 74.81.-g

## I. INTRODUCTION

Electric-field-induced carrier-doping technique, using field-effect-transistor (FET) structure or electric-double-layer-transistor (EDLT) structure,<sup>1–5</sup> attracts much attention as a new method to carrier doping, other than the methods of chemical doping. A merit of electric-field-induced doping is that we can control the doping carrier density by a gate voltage in a same sample. This will be a powerful platform in future studies of condensed matter physics. When this is used at the surface of insulators, carriers are induced near the surface, and trapped in the confinement potential of the electric field. Using enough strong field by EDLT, we can realize superconductivity of the surface metallic states at low temperature *T*, such as in SrTiO<sub>3</sub>,<sup>1</sup> ZrNCl,<sup>2</sup> KTaO<sub>3</sub>,<sup>3</sup> MoS<sub>2</sub>.<sup>4,5</sup> The gate voltage control of surface superconductivity in SrTiO<sub>3</sub> was also realized at the interface of LaTiO<sub>3</sub>/SrTiO<sub>3</sub> and LaAlO<sub>3</sub>/SrTiO<sub>3</sub>.<sup>6,7</sup>

Compared to these developments of experimental research, theoretical understandings are not enough for properties of the electric-field-induced surface superconductivity. We have to discuss whether the surface superconductivity has the same properties to those of bulk superconductivity, or whether it has different unique properties. In future experiments for unconventional superconductivity produced on a surface, we have to distinguish unique properties of surface superconductivity and exotic properties of unconventional superconductivity.

As different properties from bulk metallic states, sub-bands are formed in the surface metallic states due to the confinement potential by strong electric fields.<sup>1</sup> Since multiple sub-bands are occupied by surface carriers, this system is not ideal two-dimensional states. We also note that the local carrier density *n*(*z*) has spatial variation as a function of depth *z* from the surface in the surface metallic states, while *n*(*z*) is constant in bulk metallic states. The quantitative estimate for the *z* dependence is one of problems for the electric-field-induced metallic state. Therefore, also in the theoretical studies of surface superconductivity, we need to know detailed spatial structure of the superconducting gap in the nanoscale and its sub-band dependence. These studies enable us to find differences from bulk superconductivity.

In this letter, we study unique properties; local electronic states and sub-band dependence in electric-field-induced superconductors. We will discuss multiple-gap structure of the sub-band dependent surface superconductivity. Since we determine the spatial structure in the order of Thomas-Fermi length near the surface, we solve the Bogoliubov-de Gennes (BdG) equation<sup>8</sup> under the electric-field *F*(*z*). We discuss the depth *z* dependence perpendicular to the surface at *z* = 0. As for confinement potential *V*(*z*) by *F*(*z*), we compare two cases; triangular potential and self-consistent potential.<sup>9,10</sup> The latter is the case when induced carriers completely screen the applied electric field. The former is the opposite limit where the screening is negligible.

This paper is organized as follows. After we explain our theoretical formulation of BdG equation under electric fields in Sec. II, we study the depth-dependence of local superconducting gap structure in Sec. III, and the gap structure of the sub-band modes in the spectral weight in Sec. IV. In order to discuss the relation of sub-band dependent gap structure and the depth-dependence of superconducting states, we perform the analyses of sub-band decomposition for the surface superconductivity in Sec. V. The last section devotes to discussion and summary, including the topics of the Bardeen-Cooper-Schrieffer(BCS) - Bose Einstein condensation(BEC) crossover phenomena in the surface superconductivity.

## II. BOGOLIUBOV-DE GENNES THEORY IN CONFINEMENT BY ELECTRIC FIELD

Throughout this letter, energy, length, local carrier densities are, respectively, presented in unit of eV, nm, and nm<sup>-3</sup>. We typically consider the case of sheet carrier density *n*<sub>2D</sub> = 6.5 × 10<sup>13</sup>[cm<sup>-2</sup>], and electric field at the surface is given by *F*<sub>0</sub> ≡ *F*(*z* = 0) = 1.4 × 10<sup>-3</sup>[V/nm]. The triangular potential with this *F*<sub>0</sub> corresponds to one of the case calculated in Ref. 1 for SrTiO<sub>3</sub>, while single band case of effective mass *m*\* = 4.8*m*<sub>0</sub> is considered here. *m*<sub>0</sub> is free electron's mass.

In the normal state,<sup>1,9</sup> the eigen-energy *E*<sub>ε</sub> and wave function *u*<sub>ε</sub>(**r**) = e<sup>i(k<sub>x</sub>*x* + k<sub>y</sub>*y*)</sup>*u*<sub>ε</sub>(*z*)/√*S* are determined by

the Schrödinger equation

$$K u_\epsilon(z) = E_\epsilon u_\epsilon(z), \quad (1)$$

with

$$K = -\frac{\hbar^2}{2m^*} \frac{d^2}{dz^2} + E_{\parallel} + V(z) - \mu, \quad (2)$$

$E_{\parallel} = \hbar^2 k_{\parallel}^2 / 2m^*$ ,  $k_{\parallel}^2 = k_x^2 + k_y^2$ , and  $S$  is unit area of surface. We assume that the wave functions vanish at  $z = 0$  as the boundary condition. In the parallel direction to the surface, the eigen states are given by wave numbers  $k_x$  and  $k_y$  of plane waves. Thus, the eigen-states of Eq. (1) are labeled by  $\epsilon \equiv (k_x, k_y, \epsilon_z)$ .  $\epsilon_z$  indicates label for sub-bands coming from quantization by confinement in the  $z$ -direction. The local carrier density is calculated as  $n(z) = 2n_{\uparrow}(z)$  with

$$n_{\uparrow}(z) = \sum_{\epsilon} |u_{\epsilon}(z)|^2 f(E_{\epsilon}), \quad (3)$$

where  $f(E)$  is the Fermi distribution function. To fix  $n_{2D}$ , we tune chemical potential  $\mu$ . In the triangular potential case, the confinement potential is given by  $V(z) = |e|F_0 z$ . For the selfconsistent potential,

$$F(z) = F_0 \left( 1 - \int_0^z n(z') dz' / n_{2D} \right), \quad (4)$$

by Gauss's law, considering the screening by  $n(z)$ , and

$$V(z) = |e| \int_0^z F(z') dz'. \quad (5)$$

As  $F(z \rightarrow \infty) = 0$ ,  $n_{2D} = \int_0^{\infty} n(z') dz'$ . Iterating calculations of Eqs.(1)-(2) and Eqs.(3)-(5) in the region  $0 \leq z \leq L$ , we determine  $V(z)$  in the case of selfconsistent potential. Typically we use  $L = 80[\text{nm}]$ .

In the superconducting state, the wave function

$$\begin{pmatrix} u_{\epsilon}(\mathbf{r}) \\ v_{\epsilon}(\mathbf{r}) \end{pmatrix} = \frac{1}{\sqrt{S}} e^{i(k_x x + k_y y)} \begin{pmatrix} u_{\epsilon}(z) \\ v_{\epsilon}(z) \end{pmatrix} \quad (6)$$

is determined by solving the BdG equation<sup>8,11,12</sup>

$$\begin{pmatrix} K & \Delta(z) \\ \Delta(z) & -K \end{pmatrix} \begin{pmatrix} u_{\epsilon}(z) \\ v_{\epsilon}(z) \end{pmatrix} = E_{\epsilon} \begin{pmatrix} u_{\epsilon}(z) \\ v_{\epsilon}(z) \end{pmatrix}. \quad (7)$$

The pair potential  $\Delta(z)$  is selfconsistently calculated by

$$\Delta(z) = V_{\text{pair}} \sum_{\epsilon} u_{\epsilon}(z) v_{\epsilon}(z) f(-E_{\epsilon}) \quad (8)$$

with the energy cutoff  $E_{\text{cut}}$  of the pairing interaction. Here, we consider a conventional case of isotropic  $s$ -wave pairing. We typically use  $V_{\text{pair}} = 0.04$ ,  $E_{\text{cut}} = 0.01$ , and  $T \sim 0$ .

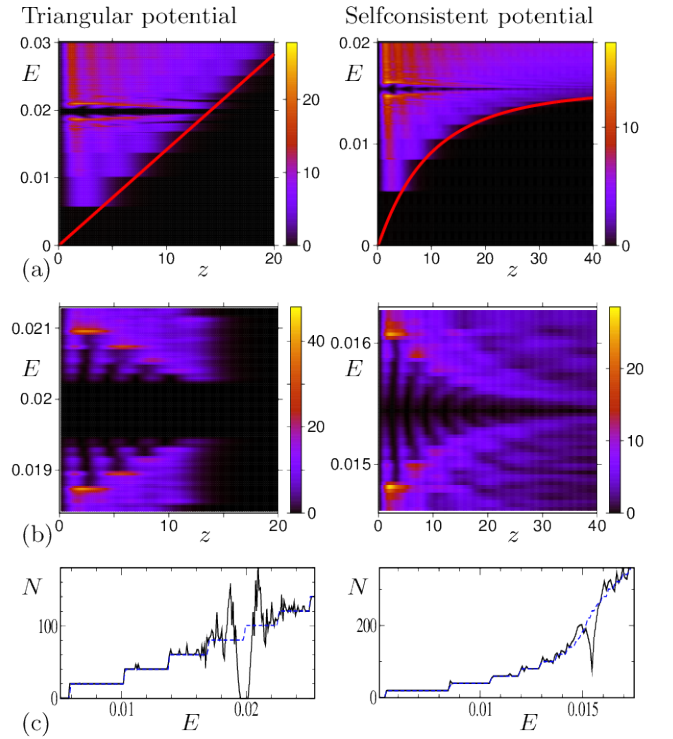


FIG. 1: (Color online) (a) Density plot of LDOS  $N(E, z)$  as a function of  $z$  and  $E + \mu$ . Solid line presents the confinement potential  $V(z)$ . (b) LDOS  $N(E, z)$  in (a) is focused near the superconducting gap. (c) DOS  $N(E)$  as a function of  $E + \mu$ . Dashed lines present  $N(E)$  for normal state. Left (Right) panels are for triangular potential (selfconsistent potential).

### III. DEPTH-DEPENDENCE OF LOCAL SUPERCONDUCTING GAP STRUCTURE

First, we study the local density of states (LDOS)  $N(E, z) = 2N_{\uparrow}(E, z)$  with<sup>11,12</sup>

$$N_{\uparrow}(E, z) = \sum_{\epsilon=(k_x, k_y, \epsilon_z)} |u_{\epsilon}(z)|^2 \delta(E - E_{\epsilon}). \quad (9)$$

The left panel of Fig. 1(a) presents  $N(E, z)$  for the triangular potential. There, we see steps of LDOS by the sub-band structure of quantized bound states, as in the normal state.<sup>1</sup> The lowest sub-band appears at  $E > E_{l=1,\min} \sim 0.0059$  near the surface. The continuum distribution above  $E_{l=1,\min}$  comes from finite  $E_{\parallel} \geq 0$ . Similarly there appears the LDOS of second sub-band at  $E > E_{l=2,\min} \sim 0.0103$ , and the LDOS of third sub-band at  $E > E_{l=3,\min} \sim 0.0138$ . Their contributions are overlapped each other at higher energies. When the sub-band level  $l$  is higher, the eigen-energy  $E_{l,\min}$  becomes higher, and the distribution spread until deeper  $z$  from the surface. The superconducting gap appears near  $\mu \sim 0.0198$ .

The  $N(E, z)$  for the self-consistent potential is presented in the right-panel of Fig. 1(a). There, we see step-structures of sub-bands at low energy region, but the step size becomes smaller at higher energy, because the slope of  $V(z)$  decreases to zero as a function of  $z$  by

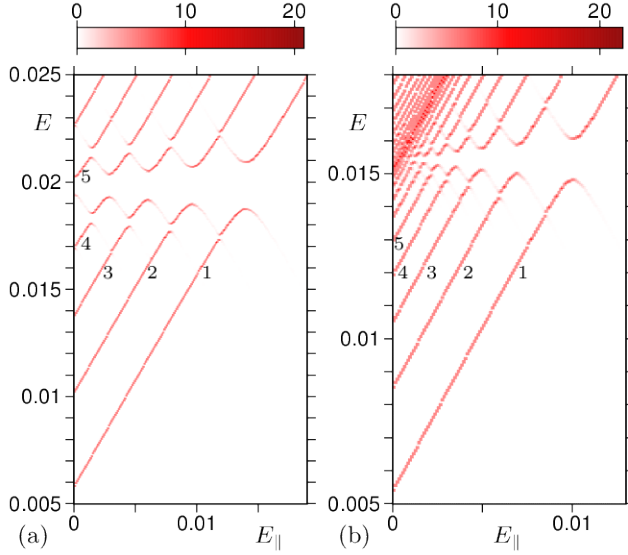


FIG. 2: (Color online) Density plot of spectral weight  $N(E, k_{\parallel})$  as a function of  $E_{\parallel} = \hbar^2 k_{\parallel}^2 / 2m^*$  and  $E + \mu$  for (a) triangular potential and (b) selfconsistent potential. Numbers in the figure indicate sub-band level  $l$ .

the screening effect. Since the chemical potential is located at  $\mu \sim V(z \rightarrow \infty) \sim 0.0154$ , occupied states with  $E < \mu$  are bound states, and empty states with  $E > \mu$  are scattering states which are free from the confinement potential. The superconducting gap opens between the bound states and the scattering states.

The superconducting gap structures are focused in Fig. 1(b). Even in the isotropic  $s$ -wave pairing, we see in-gap states which have oscillations as a function of  $z$  and steps of gap-edges as a function of  $E$ , as characteristic features of electric-field-induced surface superconductivity. High intensity peaks of  $N(E, z)$  correspond to the maximum gap-edge, whose gap amplitude decreases discontinuously with increasing  $z$ . In the selfconsistent potential (right-panel), it reduces to zero at large  $z$ .

Figure 1(c) shows density of states (DOS)  $N(E)$  after  $z$ -integration of  $N(E, z)$ . Because of the in-gap states, gap structure in  $N(E)$  is different from that of bulk isotropic  $s$ -wave superconductors. In the triangular potential (left panel), the gap-edge has width from minimum gap to gap-edge peak of maximum gap, as in anisotropic  $s$ -wave superconductors. In the selfconsistent potential (right panel), full-gap structure does not exist, since low energy states exist until near  $\mu$ . The gap shape is similar to that of anisotropic superconductors with gap nodes.

#### IV. GAP STRUCTURE OF SUB-BAND MODE IN SPECTRAL WEIGHT

We discuss that these superconducting gap structures come from the sub-band dependence of superconductiv-

ity. For the sub-band decomposition, we calculate the spectral weight  $N(E, k_{\parallel}, z) = 2N_{\uparrow}(E, k_{\parallel}, z)$  given by

$$N_{\uparrow}(E, k_{\parallel}, z) = \sum_{\epsilon_z} |u_{\epsilon}(z)|^2 \delta(E - E_{\epsilon}) \quad (10)$$

from  $N_{\uparrow}(E, k_{\parallel}, z) = -\pi^{-1} \text{Im} G_{\uparrow}(E, k_{\parallel}, z)$  with Green's function

$$G_{\uparrow}(E, k_{\parallel}, z) = \int e^{-i(k_x \tilde{x} + k_y \tilde{y})} G_{\uparrow}(E, \mathbf{r}, \mathbf{r}') d\tilde{x} d\tilde{y} |_{z=z} \quad (11)$$

$$G_{\uparrow}(E, \mathbf{r}, \mathbf{r}') = \sum_{\epsilon} \frac{u_{\epsilon}^*(\mathbf{r}) u_{\epsilon}(\mathbf{r}')}{E + i0 - E_{\epsilon}}, \quad (12)$$

and  $(\tilde{x}, \tilde{y}) \equiv (x - x', y - y')$ .<sup>13</sup> The  $z$ -integration of  $N(E, k_{\parallel}, z)$  is given by  $N(E, k_{\parallel}) = \int_0^L N(E, k_{\parallel}, z) dz$ . In Fig. 2 we show  $N(E, k_{\parallel})$ , which appear at the eigen energies  $E_{\epsilon}$ . There we see multiple parallel lines of the dispersion relation as a function of  $E_{\parallel}$ , corresponding sub-bands of surface bound states. From the bottom, the lines are assigned to sub-band level  $l = 1, 2, \dots$ , as indicated in Fig. 2. In the case of self-consistent potential, the energy distance of the dispersion relation between sub-bands decreases for higher sub-bands, and the spectral weight becomes continuous near  $E_{\parallel} \sim 0$  at  $E > \mu$  in the scattering state.

In the superconducting state, gaps open at crossing points of the particle mode and the inverted hole mode at  $E = \mu$ , forming Bogoliubov's dispersion relations of superconductivity for each level of sub-band. The superconducting gap is larger for lower sub-bands, indicating multiple-gap structure of surface superconductivity. In the case of triangular potential, the occupied lower sub-bands have different but finite gaps. In the case of self-consistent potential, sub-bands are occupied until quite higher levels, where superconducting gap reduces to zero. Therefore, the in-gap states appear until near  $E = \mu$ . As for the  $z$ -dependence of spectral weight  $N(E, k_{\parallel}, z)$ , the contribution of lower sub-band is dominant near the surface. The contributions of higher sub-bands become dominant at deeper  $z$ .

#### V. SUB-BAND DECOMPOSITION OF LOCAL SUPERCONDUCTING STATES

In Fig. 3(a), we present the local carrier density  $n(z)$  and the sub-band decomposition. The eigen-states on the dispersion relations in Fig. 2 are classified to each sub-band level  $l$ . In  $l$ -th sub-band, the wave function of the form of Airy functions has  $l - 1$  nodes along  $z$  direction.<sup>1</sup> The higher sub-band contributions can penetrate into deeper  $z$ . Since the LDOS is integrated over  $E_{l,\min} < E < \mu$  to obtain  $n(z)$ , lower sub-band contributions to  $n(z)$  becomes larger, because of smaller  $E_{l,\min}$ . The pair potential  $\Delta(z)$  and the sub-band decomposition in Fig. 3(b) have similar spatial structure to those of  $n(z)$ . It is noted that sub-band dependent pair potential becomes smaller for higher sub-bands. In the

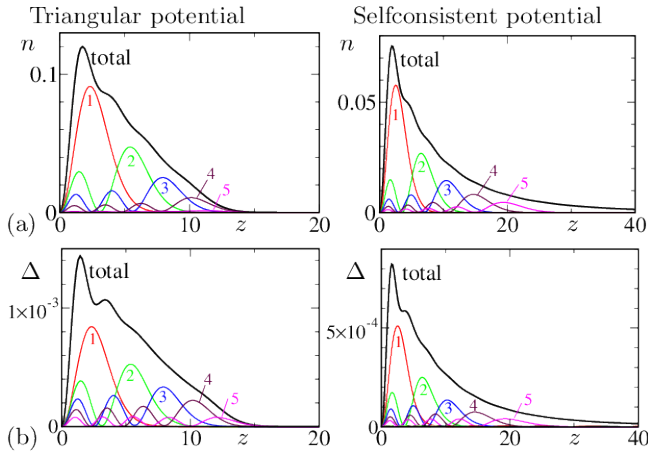


FIG. 3: (Color online) (a) Local carrier density  $n(z)$  and (b) superconducting pair potential  $\Delta(z)$  as a function of  $z$ . The sub-band decompositions are also presented for sub-band levels  $l = 1, \dots, 5$ . Left (Right) panels are for triangular potential (selfconsistent potential).

selfconsistent potential (right panels), while lower sub-band contributions are dominant,  $n(z)$  and  $\Delta(z)$  includes contributions from further higher sub-band levels  $l > 5$ . Therefore, tails of  $n(z)$  and  $\Delta(z)$  survive until deeper  $z$ .

To discuss the origin of superconducting gap structure in Fig. 1, sub-band decompositions of the LDOS are presented in Fig. 4. From Fig. 4(a), we see that lowest sub-band contribution ( $l = 1$ ) to  $N(E, z)$  has large constant superconducting gap, but its distribution is restricted in very near the surface. The contributions from higher sub-bands  $l = 2, 3, \dots$  have smaller constant gap, and the distributions spread until deeper  $z$ . By the combination of these sub-band contributions, the in-gap states and the  $z$ -dependence of superconducting gap structure in Fig. 1 are created. These sub-band contributions are clear also in the LDOS spectra in Figs. 4(b) and 4(c). There, we see multiple peaks of gap edge from sub-band contributions. Near the surface ( $z = 1.6$ ), all sub-band contributions appear, and lower sub-band contributions are dominant. Therefore the main peak corresponds to gap edge of largest gap by the lowest sub-band. In lower panels of Figs. 4(b) and 4(c) for deeper  $z$ , since lower sub-band contributions ( $l = 1$  and 2) vanish, the main peak of gap edge appears at lower gap energy corresponding to higher sub-band ( $l = 3$ ) contributions.

In addition to the superconducting gap at  $E = \mu$ , there appear extra small gaps at energies outside of superconducting gap, as seen in Fig. 2. This occurs by the crossing of the hole- and particle-modes between different sub-bands. We see these extra gaps in higher sub-band contributions also in Fig. 4(a). Because of the extra gaps, the LDOS in Figs. 4(b) and 4(c) has many extra peaks outside of the main gap energy.

We note that low-energy in-gap electronic states are not determined locally by  $\Delta(z)$  in the length order of nano-scale in this system. This is contrasted to conven-

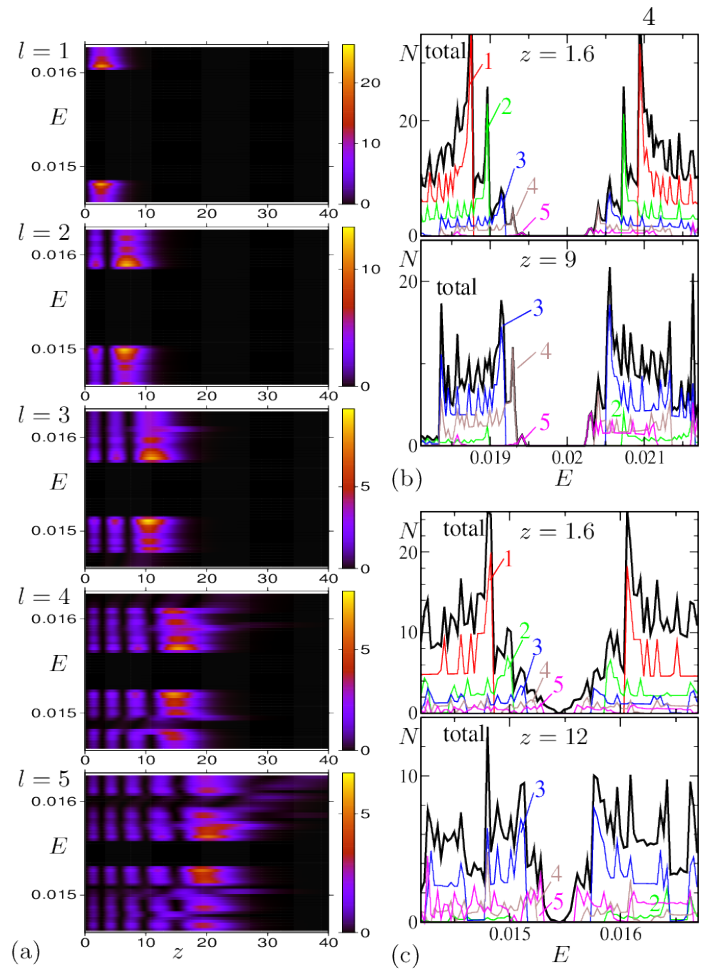


FIG. 4: (Color online) (a) Density plot of sub-band decomposition of LDOS as a function of  $z$  and  $E + \mu$  for sub-band levels  $l=1, 2, \dots, 5$  in the case of self-consistent potential. (b) LDOS  $N(E, z)$  and the sub-band decomposition at  $z = 1.6$  and 9 in the case of triangular potential. (c) The same as (b), but at  $z = 1.6$  and 12 in the case of selfconsistent potential.

tional case when  $\Delta(z)$  is suppressed in the length scale of superconducting coherence length.<sup>14–17</sup> There low-energy states appear as localized states by the suppression of the local gap. In the system of the electric field-induced surface superconductivity, approaching  $z \rightarrow 0$  near the surface,  $\Delta(z)$  is suppressed toward zero in the length order of nano-scale, as shown in Fig. 3(a). However, from Fig. 4(a), we see that localized low energy in-gap states do not appear at the surface region ( $z < 2$ ) of suppressed  $\Delta(z)$ . The local state of lowest sub-band has uniform gap with largest gap amplitude [top panel in Fig. 4(a)]. This indicates that the in-gap states reported in this paper is not due to the suppression  $\Delta(z \rightarrow 0) \rightarrow 0$ . Rather, the in-gap states comes from the deeper region, as tails of wave functions for higher sub-band levels in Fig. 4(a). This is one of intrinsic natures in the electric field-induced superconductivity.

## VI. DISCUSSION AND SUMMARY

As future experiments to confirm the in-gap states due to the characteristic multiple gap structure, we expect observations of LDOS such as by point contact tunneling spectroscopy, which will see the gap structure in upper panels of Figs. 4(b) and 4(c). The contributions of the in-gap states will be observed in experiments sensitive to DOS of the superconducting gap structure, such as magnetic resonance, optical absorptions, etc. Electric-field-induced doping will be important platform to study unconventional superconductivity. Before that, it is important to clarify the difference of properties between surface superconductivity and bulk superconductivity in conventional superconductors, as suggested in this work. As a concept of multiple-gap structure, electric-field-induced surface superconductivity can be said a new type of multi-band superconductors. We will see some similar behaviors to those of multi-band superconductors such as in MgB<sub>2</sub> and Fe-based superconductors. The number of contributing sub-bands can be controlled by the gate voltage.

We point out an interesting possibility to realize the BCS-BEC crossover phenomena<sup>18–20</sup> by controlling the gate voltage in surface superconductivity. In the cold atomic gases, the BCS-BEC crossover is seen by tuning the interaction via a Feshbach resonance.<sup>21,22</sup> The BCS-BEC crossover in multi-band superconductor was suggested by ARPES experiment in FeSe<sub>x</sub>Te<sub>1-x</sub>.<sup>23</sup> The

same situation appears in the surface superconductivity. In Fig. 2(a), the superconducting gap in 5th sub-band opens at the bottom of the band dispersion. That is, since the gap amplitude  $|\Delta|$  is larger than the Fermi energy  $E_F (\equiv \mu - E_{l=5,\min})$  from the band bottom, the BEC regime  $|\Delta| > E_F$  is realized. The gaps in other 1-4 th bands are in the BCS regime  $|\Delta| < E_F$ . As mentioned above, the gap magnitude can be tuned by the gate voltage.

In summary, local superconducting gap structure and the sub-band dependence in electric-field-induced surface superconductivity were studied by solving microscopic BdG equation. There, the in-gap states appears due to the multiple gap structure of multiple sub-band superconductivity, even for isotropic s-wave pairing. We evaluated how these structures depend on the screening condition, i.e., triangular potential or selfconsistent potential. These different characters from the bulk superconductivity, by the sub-band dependent multi-gap nature, are important to be considered, when we discuss properties of electric-field-induced surface superconductivity.

## Acknowledgements

We thank Profs. Y. Iwasa, K. Ueno, and T. Nojima for fruitful discussions, and information of their experimental results. This work was supported by KAKENHI (No. 21340103).

- 
- <sup>1</sup> K. Ueno, S. Nakamura, H. Shimotani, A. Ohtomo, N. Kimura, T. Nojima, H. Aoki, Y. Iwasa, and M. Kawasaki, *Nature Mater.* **7**, 855 (2008).
- <sup>2</sup> J. T. Ye, S. Inoue, K. Kobayashi, Y. Kasahara, H. T. Yuan, H. Shimotani, and Y. Iwasa, *Nature Mater.* **9**, 125 (2011).
- <sup>3</sup> K. Ueno, S. Nakamura, H. Shimotani, H. T. Yuan, N. Kimura, T. Nojima, H. Aoki, Y. Iwasa, and M. Kawasaki, *Nature Nanotechnol.* **6**, 408 (2011).
- <sup>4</sup> K. Taniguchi, A. Matsumoto, H. Shimotani, and H. Takagi, *Appl. Phys. Lett.* **101**, 042603 (2012).
- <sup>5</sup> J.T. Ye, Y.J. Zhang, R. Akashi, M.S. Bahramy, R. Arita, Y. Iwasa, *Science* **338**, 1193 (2012).
- <sup>6</sup> J. Biscaras, N. Bergeal, S. Hurand, C. Grossetête, A. Rastogi, R.C. Budhani, D. LeBoeuf, C. Proust, and J. Lesueur, *Phys. Rev. Lett.* **108**, 247004 (2012).
- <sup>7</sup> J.A. Bert, K.C. Nowack, B. Kalisky, H. Noad, J.R. Kirtley, C. Bell, H.K. Sato, M. Hosoda, Y. Hikita, H.Y. Hwang, and K.A. Moler, *Phys. Rev. B* **86**, 060503 (2012).
- <sup>8</sup> P. G. de Gennes, *Superconductivity of Metals and Alloys* (Addison-Wesley, Reading, MA, 1989).
- <sup>9</sup> F. Stern, *Phys. Rev. B* **12**, 4891 (1972).
- <sup>10</sup> T. Ando, A.B. Fowler, and F. Stern, *Rev. Mod. Phys.* **54**, 437 (1982).
- <sup>11</sup> M. Takigawa, M. Ichioka, K. Machida, and M. Sigrist, *Phys. Rev. B* **65**, 014508 (2001).
- <sup>12</sup> M. Takahashi, T. Mizushima, M. Ichioka, and K. Machida, *Phys. Rev. Lett.* **97**, 180407 (2006).
- <sup>13</sup> M. Ichioka and K. Machida, *J. Phys. Soc. Jpn.* **65**, 4020 (1999).
- <sup>14</sup> P.G. de Gennes and D. Saint-James, *Phys. Lett.* **4**, 151 (1963).
- <sup>15</sup> Y. Tanaka, H. Yamagami, M. Tsukada, *Solid State Commun.* **79**, 349 (1991).
- <sup>16</sup> H.K. Im, E.A. Jagla, and C.A. Balseiro, *Phys. Rev. B* **50**, 10117 (1994).
- <sup>17</sup> S. Kashiwaya and Y. Tanaka, *Rep. Prog. Phys.* **63**, 1641 (2000).
- <sup>18</sup> B. Eagles, *Phys. Rev.* **186**, 456 (1969).
- <sup>19</sup> A.J. Leggett, *J. Phys. Colloq.* **41**, 7 (1980).
- <sup>20</sup> P. Nozieres and S. Schmitt-Rink, *J. Low Temp. Phys.* **59**, 195 (1985).
- <sup>21</sup> M.W. Zwierlein, J.R. Abo-Shaeer, A. Schirotzek, C.H. Schunck, and W. Ketterle, *Nature* **435**, 1047 (2005).
- <sup>22</sup> S. Jochim, M. Bartenstein, A. Altmeyer, G. Hendl, S. Riedl, C. Chin, J.H. Denschlag, and R. Grimm, *Science* **302**, 2101 (2003).
- <sup>23</sup> Y. Lubashevsky, E. Lahoud, K. Chashka, D. Podolsky, and A. Kanigel, *Nature Phys.* **8**, 309 (2012).